Experimental investigation of large-scale high-velocity soft-body impact on composite laminates

A D Cochrane, Joël Serra, J K Lander, I K Partridge, H Böhm, T Wollmann, A Hornig, M Gude, S R Hallett

International Journal of Impact Engineering 161 (2022) 104089

Contents lists available at ScienceDirect

International Journal of Impact Engineering

journal homepage: www.elsevier.com/locate/ijimpeng

Experimental investigation of large-scale high-velocity soft-body impact on composite laminates

A.D. Cochrane [a], J. Serra [a], J.K. Lander [b], I.K. Partridge [a], H. Böhm [c], T. Wollmann [c], A. Hornig [c], M. Gude [c], S.R. Hallett [*,a]

[a] Bristol Composites Institute (BCI), University of Bristol, United Kingdom
[b] Rolls-Royce plc, United Kingdom
[c] Institute of Lightweight Engineering and Polymer Technology (ILK), Technische Universität Dresden, Germany

A B S T R A C T

High-performance aerospace laminated composite structures manufactured from carbon-fibre prepreg are very susceptible to delamination failure under in-flight impact conditions. Much testing has been conducted at small length scales and quasi-static strain-rates to characterise the delamination performance of different material systems and loading scenarios. Testing at this scale and strain-rate is not representative of the failure conditions experienced by a laminate in a real impact event. Full-scale testing has also been conducted, but much of this is not in the open literature due to intellectual property constraints. Testing at this scale is also prohibitively expensive and involves complex failure mechanisms that cause difficulty in the analysis of associated failure behaviour. A novel test is presented which provides a simple, affordable alternative to full-scale testing but which invokes failure at sufficient scale and velocity to be representative of real component failure. This test design is experimentally validated through a series of soft-body gelatine impact tests using a light gas-gun facility. A fractographic analysis using scanning-electron microscopy was undertaken to examine microscopic failure behaviour, showing a possible reduction in crack mode-ratio during propagation.

1. Introduction

The use of carbon-fibre reinforced plastic (CFRP) in aerospace structures is now widespread and allows component manufacturers to achieve enhanced and tailored properties while simultaneously reducing weight. CFRP materials are increasingly being deployed in the most high-performance of applications such as in rotating gas-turbine engine components [1]. A major drawback of such materials is that whilst they offer very high stiffness, they are relatively brittle [2]. Energy absorption mechanisms are therefore different from those of more ductile materials such as metals, with a significant example being that of interlaminar crack formation through a process known as delamination. Composite components are particularly susceptible to delamination under impact conditions such as during bird-strike [3,4]. Delaminations may propagate in a rapid and unstable manner throughout a composite structure and cause significant reductions in residual structural stiffness, leading to potentially catastrophic in-flight events if left unchecked. Composite structures are now being designed and produced to have improved levels of damage tolerance, measurable by the ability of a structure to reduce progressive crack growth and thus improve their resilience to structural failure [5]. A contributing factor to this improved damage tolerance are advances in material technology, such as the inclusion of thermoplastic particles embedded in the matrix resin [6].

The damage tolerance of a carbon fibre pre-preg laminate is defined predominantly by the interlaminar fracture toughness, a property governed by the neat matrix resin which constitutes the interface between the fibrous ply layers. Its strength is substantially lower than that of the fibres, and so is a limiting factor in the impact performance of laminated prepreg-manufactured aerospace structures where there is a lack of fibrous material in the through-thickness direction. The interlaminar fracture toughness of composite laminates is most commonly characterised at coupon level and at quasi-static strain-rates through a series of standard tests representing different loading conditions. The established test types are double-cantilevered beam (DCB) [7] for Mode I, end-loaded split (ELS) [8] and end-notched flexure (ENF) [9] for Mode II and mixed-mode bending (MMB) [10] for mixed-mode. More recently, such tests have been extended to include through-thickness reinforcement (TTR) such as Z-pins to assess reinforced fracture toughness [11], but the modified test methods are not yet formalized in any standard. Fracture toughness tests such as those described generally involve loading specimens of fixed geometry, boundary conditions and loading or displacement extents and rates to benchmark interlaminar properties between different material systems under common circumstances.

The need for a sub-element scale test in which large delaminations

* Corresponding author.
E-mail address: stephen.hallett@bristol.ac.uk (S.R. Hallett).

https://doi.org/10.1016/j.ijimpeng.2021.104089
Received 13 May 2021; Received in revised form 14 October 2021; Accepted 20 November 2021
Available online 30 November 2021

are developed is highlighted by the case of Z-pin TTR, which is used to reinforce the interlaminar regions in laminates made from pre-impregnated material (pre-preg). It has been established that in order to test the efficacy of Z-pin TTR in arresting crack propagation, a Z-pin array must encounter a crack over sufficient distance and thus be implemented in a structure of sufficient scale to invoke *large-scale bridging* of that array [11–13]. During large-scale bridging the crack becomes large enough to cause pins to 'bridge' the fracture surfaces over sufficient distance to generate the maximum possible bridging force to suppress further propagation (Fig. 1). At the fracture toughness coupon test scales described previously, such large-scale bridging behaviour is not possible. In a full-scale impact event, such as on an aircraft structural component at take-off speed, the delaminations produced will likely be large in scale and occur at high velocity. Full-scale industrial gelatine impact testing has been conducted to evaluate the effect of this type of event, but such testing is prohibitively expensive, performed on complex geometry and produces sophisticated failure mechanisms that are difficult to isolate and analyse [14–16]. Data on recent testing at this scale is also not available in the open literature due to intellectual property constraints. A simple, affordable and laboratory-scale test is thus required which yields delamination failure of sufficient scale - in this case described as *large scale* - to invoke large-scale bridging, takes place at high enough velocity to be representative, and which uses a specimen of basic geometry which may be readily modelled and simplified for analysis purposes.

The closest emulation of high velocity, large-scale delamination conditions in a laboratory-scale test has been the Soft-Body Beam-Bending (SBBB) test, which was developed as a representative analogue to reproduce loading conditions observed in a full-scale component under impact but in a much smaller specimen and rig [18] (Fig. 2). With high levels of bending allowed under a normal soft-body impact, the intended failure mode was a large primarily Mode II delamination starting from a single pre-crack, inserted at the mid-plane and mid-span of the laminate. The SBBB method is a very relevant example of a test which has been developed to induce a specific type of failure and avoid failures which will negatively affect the tests ability to be representative (i.e. produce delamination without fibre failure). The test parameters used, for example the test velocity range of 100 - 200m /s, have been specifically selected to reproduce loading conditions observed in a real aerospace component in-flight at take-off and landing forward speeds. The test has been conducted on Z-pinned laminates to investigate the Mode II capability of normally-aligned carbon-fibre Z-pins under soft-body impact [19]. However, it was found that the SBBB test method was still insufficient to produce large-scale bridging in an array of Z-pins. The current study therefore aims to produce a novel test standard which eliminates the described shortcomings.

An example of a larger-scale sub-element type test used to demonstrate the impact damage performance of different materials systems at high velocities was presented by Hou and Ruiz [20]. The presented test method is one of the few large sub-element type tests on a composite structure which makes use of soft-body impact, a cantilevered-type test specimen and investigates delamination behaviour at high velocity presented in the literature to date. Other studies, such as in [21], have examined impact on cantilevered plates but where the projectile was 'sliced' by the leading edge of the specimen to represent impact of a gas-turbine rotating engine component. For the current study, full surface impact was more suitable to generate greater bending and resulting delaminations, with fewer unknowns and variability, such as slice length. Use of full surface impact also allowed for quantification of the exact amount of kinetic energy transmitted to the plate during testing. In [20], cylindrical gelatine projectiles were fired at composite laminate flat plates of in-plane dimensions 216 × 102mm near the leading edge at the mid-span point and at an angle of 40° to the laminate surface (Fig. 3a). The length of laminate which sits under the clamping fixture is notable - which is just over 10% of overall laminate length. The laminates were subjected to impact at speeds between 200m/s and 300m/s, and the gelatine velocity was measured by high-speed camera. The laminate damage was then measured via ultrasonic C-scan after the testing. For some tests, projectile mass was altered by increasing projectile length while maintaining diameter. The research in [20] outlined the ability to change failure modes by altering projectile mass - it was found that larger masses at lower velocities initiated damage from the root (Fig. 3b) region, while high velocities and small masses produced local failure near the impact zone (Fig. 3c).

It can be identified that although composites' delamination is well characterised at coupon scale by numerous studies in the literature, there is a gap in bridging smaller length scales to full structural component scale. It is particularly the case for high-rate, soft-body impact behaviour where component performance can not be assumed to be the same as that observed in coupon tests. The current study has therefore set out to achieve the following:

- A novel soft-body impact test which employs a large-scale specimen geometry relative to that used in the SBBB test (in-plane dimensions 200mm × 20mm) [18] and produces a large, scalable delamination in the laminate; the in-plane dimensions should not fall below the largest example currently observed in a delamination test (216mm × 102mm in [20]);
- A test suitable for high velocities, via impact loading, in order to provide representative loading conditions of a real in-flight impact, which would occur at an impact velocity of between 100m/s and 200m/s;
- A test specimen suitable for through-thickness reinforcement (TTR) e.g. (Z-pins);
- A test that allows for variation in the amount of damage, and ideally failure behaviour, through modification of the impactor configuration in terms of velocity, incidence angle and impact location.

2. Test development

The general strategy used in the production of the final test design is outlined here along with justification for each of the design decisions in terms of specimen geometry and projectile impact profile.

Given the objectives outlined in Section 1, soft-body gas-gun testing was selected as the test method as it is capable of meeting these requirements. The use of a soft-body gas-gun impact test allowed for sufficient velocities between 100-200m/s and corresponding failure conditions to be representative of an impact during take-off or landing phases of forward flight. For simplicity, the specimen would not be subjected to any static preload (to simulate centrifugal forces) prior to impact. Based on the observations from the Soft-Body Beam Bending (SBBB) behaviour [19], a test was required which allowed for delamination propagation across a larger area, with a more varied form of delamination possible (ideally across a range of mode-ratios). Using a cantilever-type test format gives versatility afforded by only a single end being clamped. If a cantilevered design was used, then the amount of

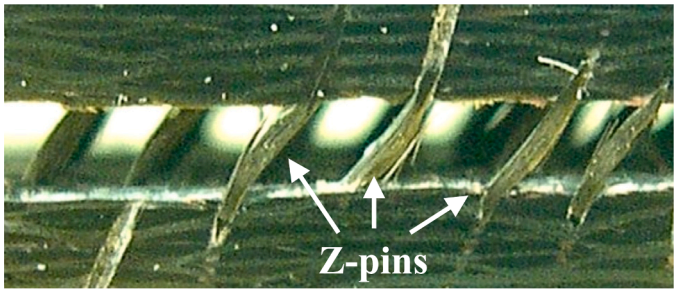

(a)

Fig. 1. Mixed-mode crack-bridging by an array of Z-pins through-thickness reinforcement [17].

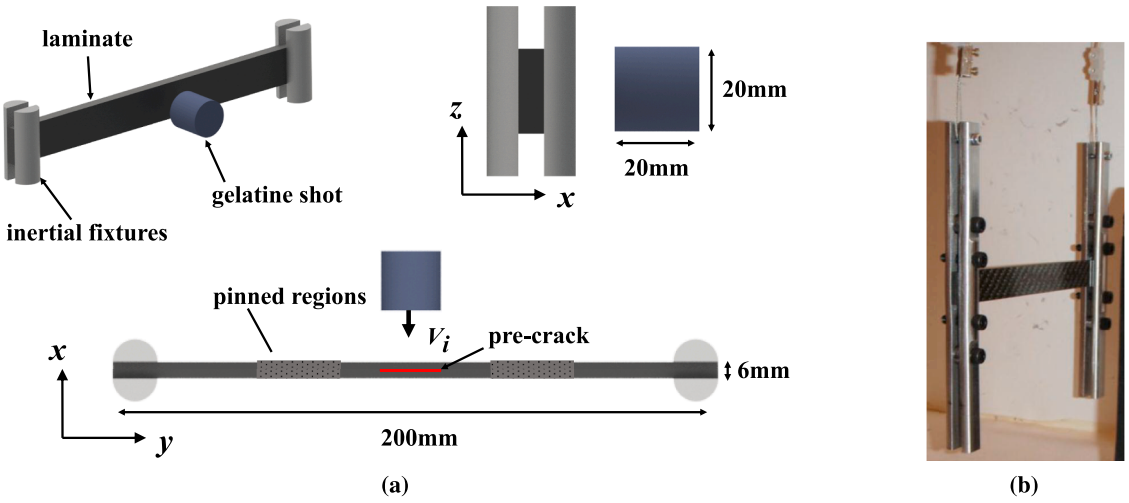

Fig. 2. (a) shows an illustration of the test design and geometry for the Soft-Body Beam-Bending (SBBB) test, and (b) shows a photograph of the experimental setup [19].

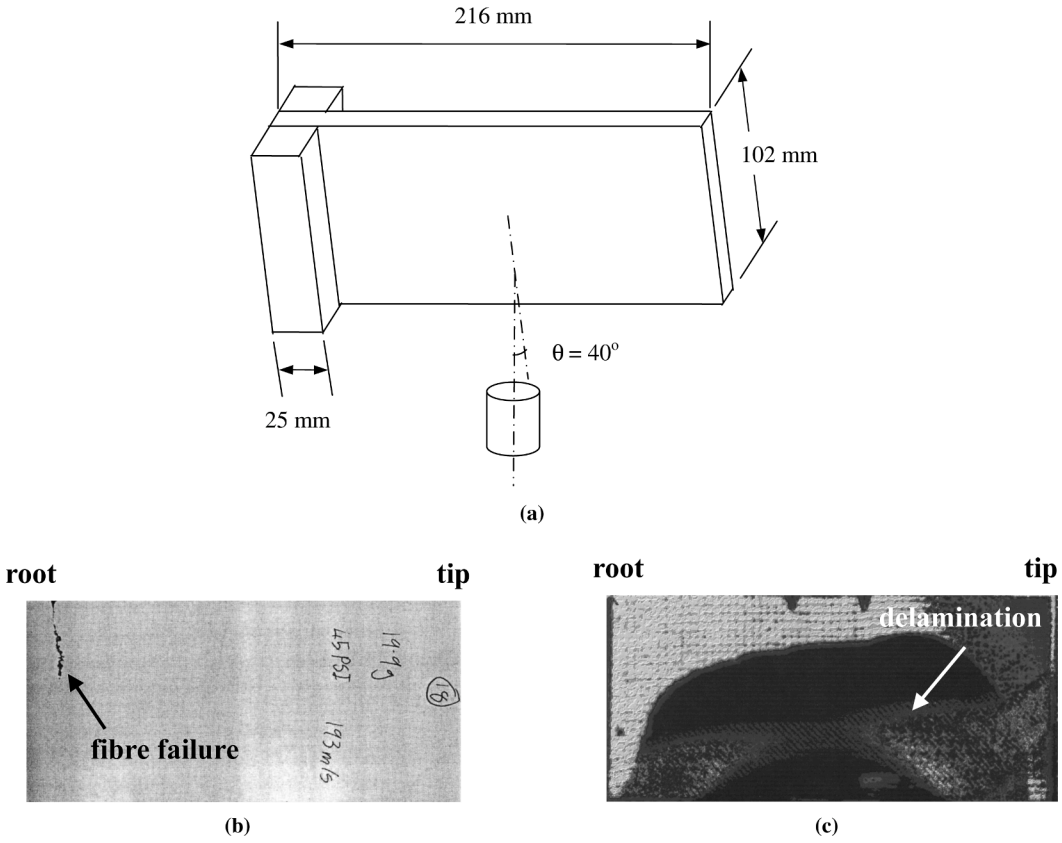

Fig. 3. (a) Configuration of the cantilevered gelatine impact test outlined in [20]; (b) C-scan result from a Fibredux 914C-713-40 plate with a higher-mass (19.9g) lower-velocity (193m/s) projectile, and (c) C-scan result from an AS4/PR520 plate using a lower-mass (10g), higher-velocity (306m/s) projectile.

plate bending and twist generated could be varied by modifying the impact location of the projectile on the specimen surface. It was therefore proposed that one end of the current test specimen be left unconstrained i.e. the specimen would be in a cantilevered configuration (Fig. 4) in order to give the greatest versatility in bending deflections generated. Since a large surface area was also desired across which delaminations could propagate, the test made use of a specimen of sufficient width rather than a very narrow beam (Fig. 5). In order to generate sufficient bending under impact loading to give a high probability of generating delamination cracks, the aspect ratio was set above $L_x/L_y =$ 1.5 - where L_x and L_y are specimen length and width dimensions respectively - such that the specimen had at least 50% more length than width. The available manufacturing in-plane bed-size was limited to 300mm x 250mm for implementation of Z-pins - in a later study. Based on these considerations, a final specimen in-plane geometry of 290mm x 180mm was set.

The test was aimed to balance the 0° ply compressive stresses in the root region with the delamination observed in the laminate. It was necessary to achieve a large amount of delamination - ideally on a single, primary delamination interface - while maintaining stress levels which

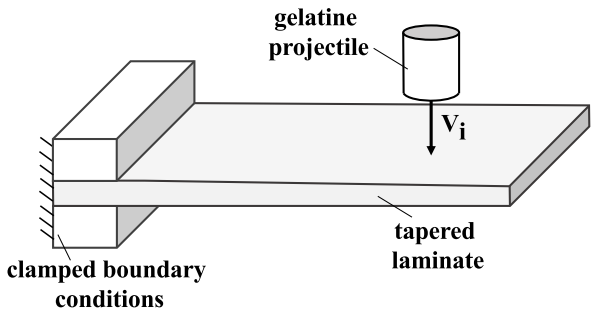

Fig. 4. Basic form of the test concept: a cylindrical gelatine projectile is fired axially at a tapered, cantilevered composite laminate which is clamped between two end-plates.

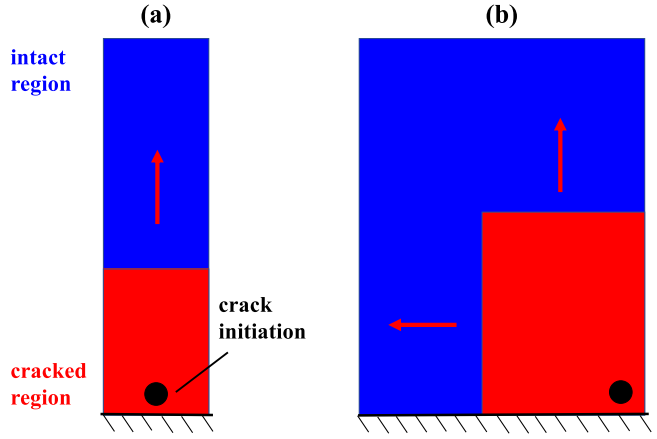

Fig. 5. Illustration of the effect of increasing surface area on the potential crack propagation behaviour: (a) shows a narrow specimen, in which the crack propagates only in a single direction, but (b) shows a wider specimen where the crack may propagate in at least two directions.

did not cause substantial risk of fibre failure. There were thus two main risks associated with the test design:

Risk 1: *No delamination*, where the test failed to produce any delamination or delamination of insufficient scale to be useful;

Risk 2: *Fibre failure*, where the specimen underwent such significant bending that substantial fibre failure - possibly resulting in full section-failure of the specimen - occurred near the root.

It was necessary to develop enough bending to cause crack initiation and propagation, but with minimisation of any fibre failure near the root. It was therefore proposed to taper the laminate via lengthwise ply-drops to allow for a large thickness near the root (to provide root strength) and a smaller thickness near the tip (to encourage bending) such that both requirements were met. To maintain a simple design with reduced manufacturing costs, the taper was single-sided such that one surface was flat. A uniform-thickness region was retained near the root where the specimen was to be clamped into the root fixture. Specimen width, thickness and taper ratio were configured to generate test behaviour fulfilling the objectives described above. To achieve a high root-strength, the IM7/8552 laminate was defined by a bespoke layup which was 0°-dominated but contained features such as blocked continuous plies and orientation differences of 90° between adjacent plies to promote the required delamination. A single 4 ×4 plain-weave M21/IMA woven ply was included on each surface to provide impact protection to the underlying UD plies. The layup is illustrated in Fig. 6.

In terms of the projectile, a gelatine impactor of cylindrical axial profile was used (Fig. 4). The selected light gas-gun had a bore of 70*mm*, and the gelatine mould used gave a projectile of the geometry shown in Fig. 7. The rounded nose was designed so that any slight misalignment would not have a great effect on the delamination results (as observed with the flat-fronted projectile in the SBBB tests). The lengthened body relative to diameter would give a sustained pressure pulse on the laminate surface and encourage greater bending, and the axial shot would provide a small projectile footprint which would allow for greater degree of variation in the impact location depending on the test requirements. The projectile impact location (off-axis and near the laminate tip) was selected to generate a substantial amount of bending and twist, and the incident angle (15° to the surface of the laminate) was chosen to control the flow of gelatine across the surface after impact.

For boundary conditions, it was proposed that the test specimen be clamped between two plates with clamping pressure provided by torque bolts. The clamped length of laminate was set at $l_c = 30mm$, based on a clamping length of approximately 10% laminate length in prior work [20]. Fibre-failure at the plate roots was avoided by using a radius ($r_c = 15mm$) on the clamping blocks to prevent stress concentrations. Taking all of the above test design choices and limitations into account, the resultant test design is outlined in terms of geometry by Fig. 8. It should be noted that the experimental configuration presented in this study that produced the desired large-scale delamination result is specific to this particular material, geometry and test parameters. Alteration of the test parameters and configuration may induce other failure modes such as fibre failure, particularly at the cantilever root.

3. Manufacture & testing

3.1. Specimen manufacture

Six specimens were manufactured for gas-gun impact testing. The specimen was designed using a simple geometry in order to minimise manufacturing costs. It used one-dimensional, single-sided taper and was manufactured using hand-layup using from unidirectional (UD) IM7/8552 pre-preg material with an M21/IMA wovenpre-preg surface protective layer. In order to facilitate simple manufacturing, soft top tooling was employed such that complex tooling parts did not require machining at considerable expense. A silicone sheet was placed on top of the laminate above the release film and beneath the vacuum bag, and also beneath the laminate between the release film and the tool plate (Fig. 9). The use of silicone sheet was in order to maintain consistency with the manufacture of Z-pinned laminates which would be the subject

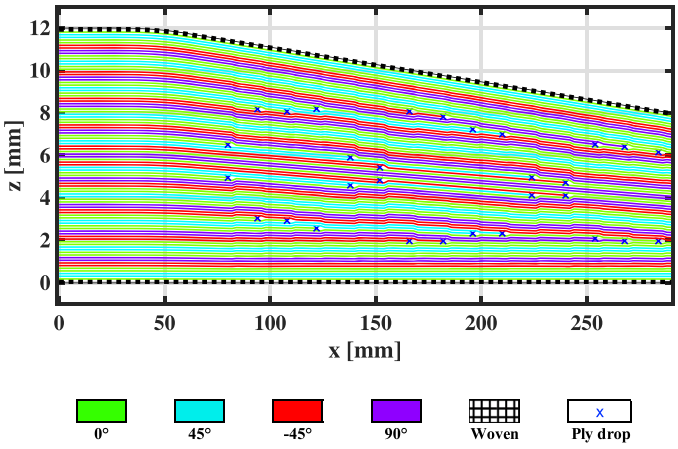

Fig. 6. Illustration of the tapered laminate layup, showing the woven ply on the upper and lower surfaces and with locations of ply terminations highlighted.

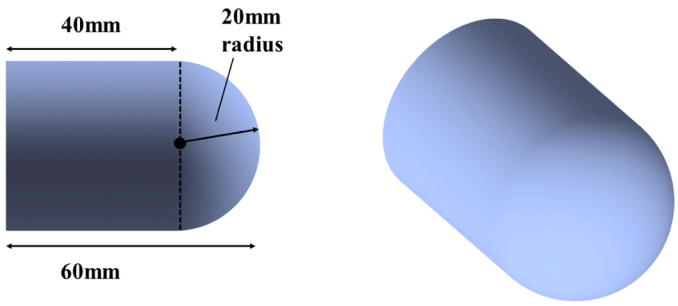

Fig. 7. 'Rounded cylinder' projectile design, showing key dimensions.

of a further study.

Specimens were cured using a standard IM7/8552 aerospace autoclave curing cycle [22]. The laminates were then de-bagged and trimmed to the designed in-plane dimensions using a water-jet cutting facility. Specimen thicknesses were measured at several points; specific data regarding specimen thickness is presented in Section 3.3.

3.2. Experimental setup & test method

The design process resulted in a test configuration which produced a bending response in a tapered, cantilevered composite plate that was sufficient to initiate delamination near the root without inducing fibre failure. The test was sized and tailored to produce the desired result within physical constraints of available equipment and manufacturing facilities. The manufactured specimens were subjected to high-speed gelatine gas-gun impact testing to generate results for the study of large-scale delamination propagation at high rate.

The test made use of a light gas-gun facility (Fig. 10)) which was used to accelerate a gelatine projectile within a foam sabot to impact velocity. The gas-gun had a gun bore of 70*mm*. The gelatine was made via an aqueous solution of powdered ballistic gelatine and water (Fig. 11a). The sabot was manufactured from polyurethane foam inside a closed mould and sanded to remove unfavourable surface roughness or imperfections, subsequently greased by hand and rammed to its firing position at the base of the barrel (Fig. 11b).

The specimen clamping assembly was designed and built by TU Dresden and the technical design is shown in Fig. 12. Eight *M*10 bolts connected the two clamping plates and were used to apply clamping pressure to the specimen surfaces. The entire test fixture was located within an impact-resistant metallic chamber which contained transparent plastic windows to allow for viewing and high-speed camera recording of the impact event. The as-manufactured tapered composite beams were mechanically clamped into the fixture at the flat, thick root end and the clamping bolts were initially hand-tightened followed by application of a precise torque of 30*Nm* using a torque-wrench. The enclosure had a removable lid which was bolted in place using a pneumatic drill. The pressure vessel was pressurised to a prescribed

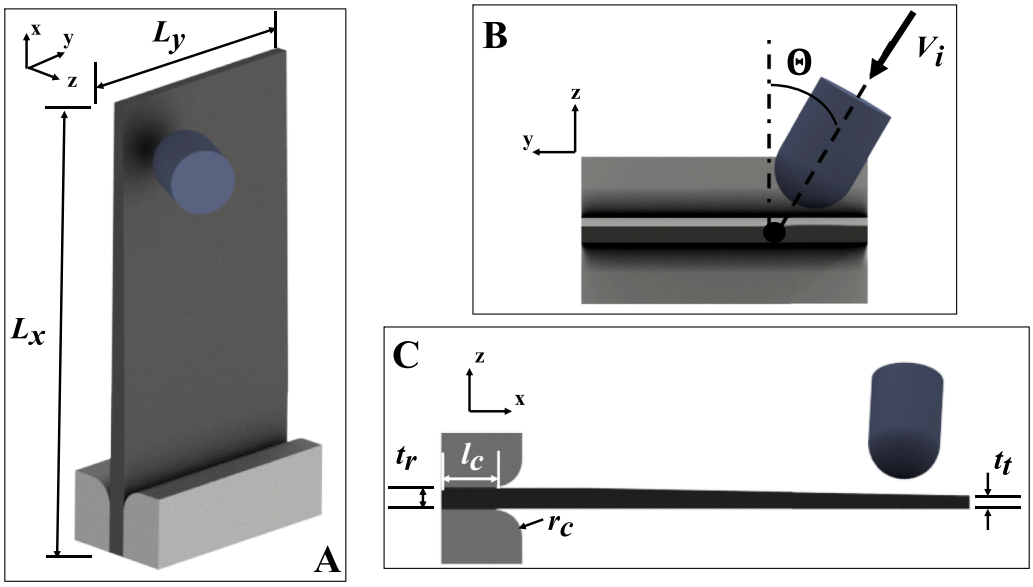

Fig. 8. Top) Schematic representations of the final test configuration: A) Isometric; B) viewed along $x-$ axis and C) viewed along $y-$ axis schematic representations of the final test configuration; Bottom) the numeric values for key parameters associated with the final design, where (px,py) are the $x-$ and $y-$ co-ordinates of impact relative to the specimen edges at $x = 0mm$ and $y = 0mm$ on the impact side; d_i is the diameter of the nose of the impactor; l_i is the total length of the impactor; m_i is the nominal mass of the impactor; l_c is the clamped length of the laminate in the $x-$ direction, and r_c is the radius of the fillet on the fixture edge contacting the laminate.

L_x [mm]	L_y [mm]	t_r/t_t	t_r [mm]	V_i [m/s]	Θ [°]	(p_x, p_y) [mm, mm]	d_i [mm]	l_i [mm]	m_i [g]	l_c [mm]	r_c [mm]
290	180	3/2	12	145	15	(270,20)	40	60	62	30	15

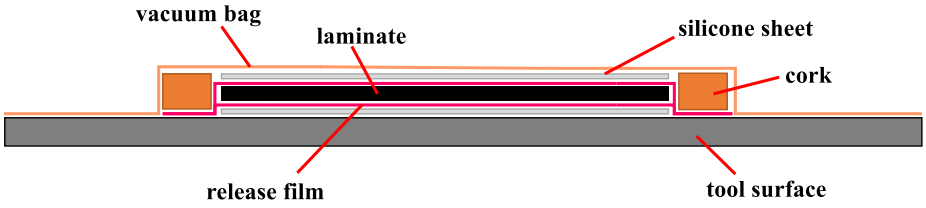

Fig. 9. Schematic diagram of the vacuum-bagging configuration for each laminate, showing use of 3*mm* silicone sheeting between the upper laminate surface and the vacuum bag, and lower laminate surfaces and tool-plate.

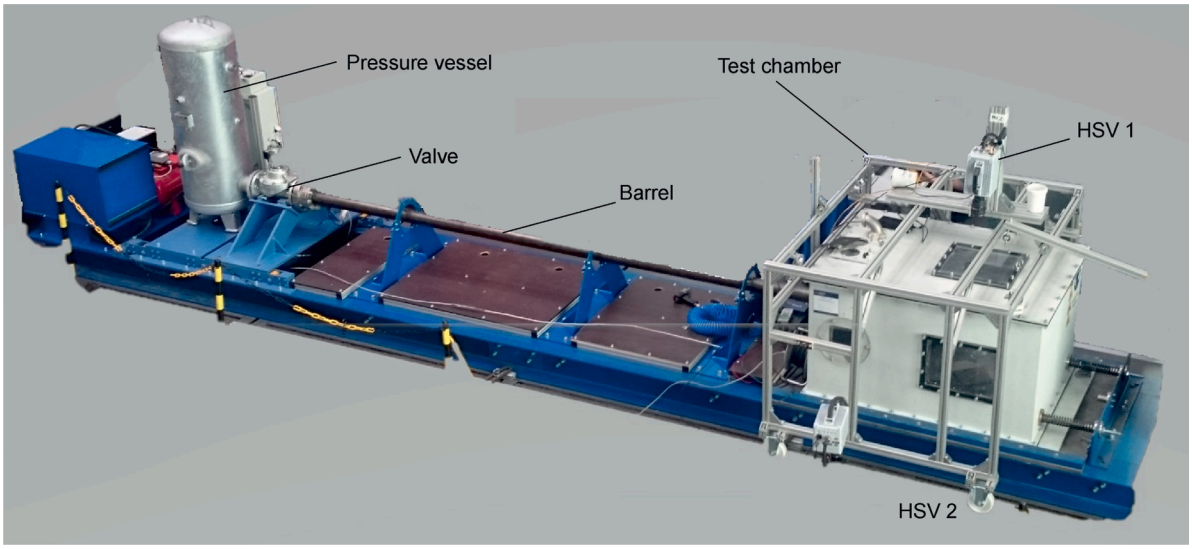

Fig. 10. Photograph of gas-gun configuration with key components indicated.

(a) (b) (c)

Fig. 11. (a) Rounded-end gelatine shot post-trimming and pre-marking for firing; (b) Foam sabot post-sanding and pre-greasing for firing; (c) Gelatine with nose painted placed into sabot before being placed into firing position.

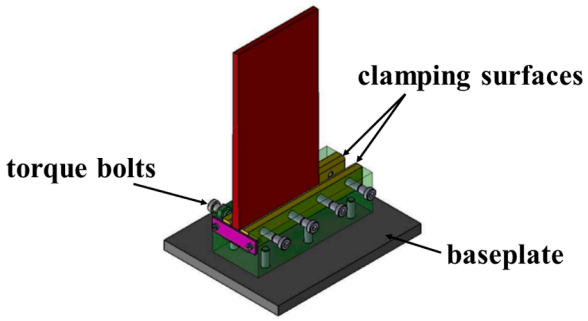

Fig. 12. CAD drawing of the test fixture assembly, showing the arrangement of the *baseplate* and *clamping mechanism* with respect to the *laminate position*.

value based on prior calibration in order to generate the correct projectile velocity on firing. Trial shots were conducted against a dummy steel plate to verify the gelatine velocity and shape. The test environment was not temperature-controlled or under vacuum, and the tests took place in ambient environmental conditions - though temperature was monitored to ensure the tests took place at approximately normal room temperature ($25^{\circ}C$)

Quantitative measurements of projectile velocity and specimen deflections were taken through two Photron FASTCAM SA4 high-speed cameras running at 25,000fps. The cameras were positioned orthogonal to the short tip-face of the laminate (*HSV1*) and orthogonal to the long edge furthest from impact (*HSV2*) as illustrated in Fig. 13. Figure 13c and d show approximately the view seen through each high-speed camera. Scale-bars are visible orthogonal to the view for *HSV1* (Fig. 13) allowingc for accurate calculation of both impact velocity and tip deflections in postprocessing via known scale lengths. Prior to impact, specimens were coated in matt white paint and marked with a series of lines and dots (configuration shown in Fig. 14) to allow for easier measurement of deflections and crack propagation. Use of white paint allowed cracks to be visualised along edges. Dots were used to aid in tracking of the two sub-laminates after delamination near the mid-plane. The coating used was a solvent-based alkyd paint.

Six specimens were tested using the test design parameters. The design process intended to reduce or prevent the need for the many trial tests which could precede full testing at the optimal set of parameters by eliminating the need to tune experimental parameters. Experimental trials are costly and introduce the risk of being unable to obtain the optimal set of parameters in the set amount of time or number of specimens available. During the design phase, an initial test velocity of $V_i = 145m/s$ was selected to attempt to generate an initial delamination near the root and close to the laminate mid-plane by global bending and propagate the delamination through structural deflections. Delamination extent in all cases was measured using ultrasonic C-scanning. Specimens were C-scanned using an air-coupled ultrasonic scanning system before and after each test. Crack propagation was also observed via tracking the crack tip along the long edge using *HSV2*. Specimen

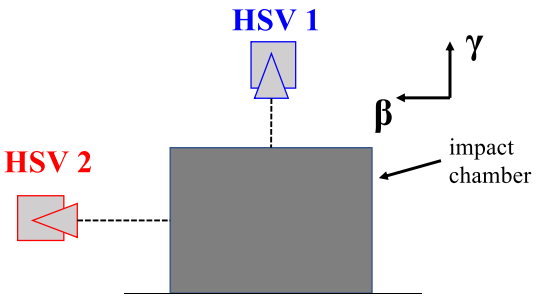

(a) Schematic diagram of high-speed video camera (HSV) configuration viewed along gas-gun α−axis, showing *HSV1* above impact chamber pointing vertically downwards (in β−direction) and *HSV2* pointed orthogonally at the long edge of the specimen

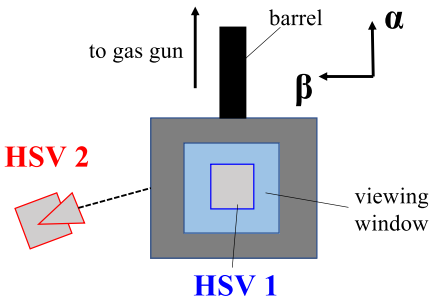

(b) rotated version of diagram (a) viewed along the gas-gun γ-axis

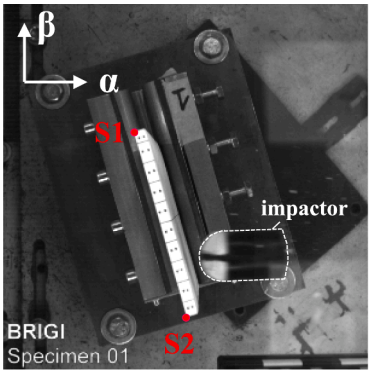

(c) Still from *HSV1* showing displacement measurement points *S1* and *S2*

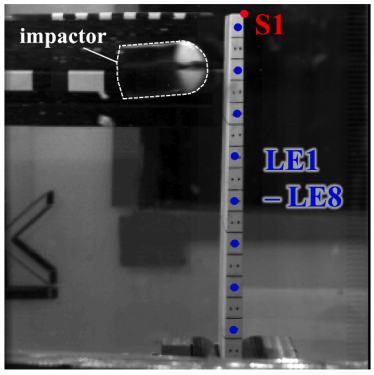

(d) Still from *HSV2* showing displacement measurement points *S1* and *LE1-LE8*

Fig. 13. High speed video camera setup; a) end view, b) top view, c) representative image from HSV1, and d) representative image from HSV2.

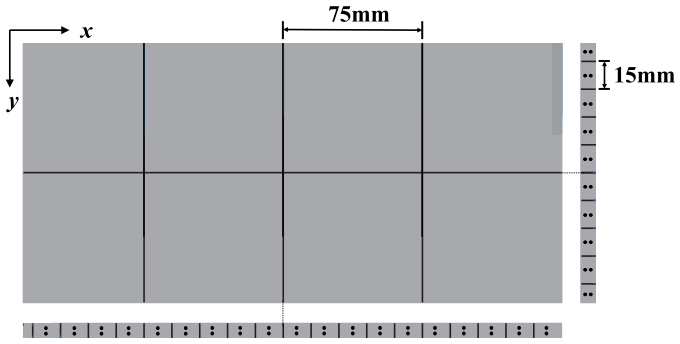

Fig. 14. Sketch of the mark-up configuration on the laminate surface, showing location of lines and dots. Two end-projections are shown on the *bottom* and *right* of the base diagram, which shows the laminate upper surface. Taper has been omitted for clarity.

deflections and gelatine behaviour were observed using both *HSVs*.

3.3. Results

Table 1 summarises the test results. The average measured root and tip thicknesses are given, with an average root thickness of $t_r = 12.7mm$ (6.2% over nominal) and tip thickness of $t_t = 9.0mm$ (13.1% over nominal). The average gelatine mass is 71.4g, which is approximately 20% over the nominal gelatine mass due to the experimental gelatine used. The initial test velocity based on finite element analysis was set at $V_i = 145m/s$. This was intended to initiate delamination near the root and also propagate it sufficiently such that, were through-thickness reinforcement present, the delamination would be sufficient to examine the effect of the reinforcement. For the test *CP1*, the result was satisfactory; however, the repeat test *CP2* did not produce sufficient delamination, and so test velocity was increased across tests *CP3* and *CP4* until substantial delamination was achieved again. A large amount of delamination occurred in test *CP4*, at a new test velocity of $V_i = 164.8m/s$. Due to this producing a satisfactory delamination result, the test velocity set-point thereafter was set at $V_i = 165m/s$. An average delaminated area A_d of 80% ($CoV = 0.231$) was measured for all tests at

Table 1
Results for the unpinned gelatine impact tests.

Specimen ID	Tip thickness [mm]	Root thickness [mm]	Gelatine mass [g]	Velocity [m/s]	Impact Energy [J]	A_d [%]
CP1	9.0	12.8	70.4	145.0	740.2	47
CP2	9.1	12.8	71.8	145.0	754.9	24
CP3	9.1	12.9	73.3	154.0	880.4	25
CP4	9.0	12.7	70.0	164.8	950.4	64
CP5	9.0	12.7	71.9	166.1	992.1	75
CP6	9.1	12.8	71.3	165.2	972.2	100

a nominal velocity of $V_i = 165m/s$. Firing velocity was achieved across all tests to within $\pm 2.5ms$ of nominal.

3.4. Experimental observations

3.4.1. Impact response

HSV footage was examined to determine the dynamic response of the specimen, in terms of general behaviour after impact, measured deflections and crack propagation. Figure 15 shows a typical deflection profile observed from *HSV1* and *HSV2*, and Fig. 16 shows a more detailed sequence of images illustrating longitudinal bending and crack progression from *HSV2*. It is clear that the specimen undergoes substantial longitudinal and twisting deflections, and that delamination initiation and propagation is driven by global bending deflections of the laminate.

While it is difficult to ascertain exactly where delamination initiates, it is likely that the initiation point is in the root region farthest from the impact location where intuitively there is the greatest amount of interlaminar shearing due to high levels of both bending and twisting. Delamination initiation will likely either occur during the initial downward twisting deflection (Fig. 15b and c) immediately after impact or on the reversed twisting deflection (Fig. 15c and d).

After initiation, the majority of crack propagation appears to occur rapidly during the reversed transverse deflection (Fig. 15c and d and between Fig. 16a and b). Crack propagation rate is estimated from the *HSV2* footage to be in the order of $V_c = 150m/s$. The plate appears to remain deflected away from the impact for some time while the crack propagates. The sustained pulse of bending coincides with crack propagation, suggesting that the plate is losing stiffness during cracking. The gelatine clearly flows from one side of the specimen, across the width and then continues across the surface of the specimen in a chordwise manner until it departs the specimen surface (Fig. 15). An interesting observation is that while the gelatine appears to flow in a fluid-like manner in the high-speed video footage (e.g. in Fig. 15), the retrieved fired gelatine obtains much of its pre-impact mass and largely remains as a single continuous structure (Fig. 17).

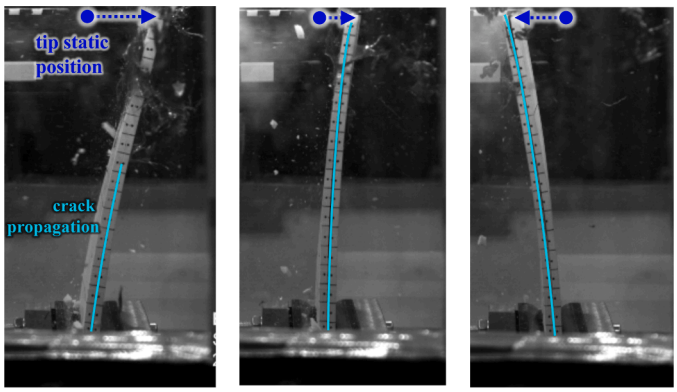

(a) time = $3ms$ **(b)** time = $5ms$ **(c)** time = $8ms$

Fig. 16. Typical deflection time sequence during crack propagation showing movement of the (nearest) tip in the *HSV2* footage for case *CP6* with $V_i = 165m/s$.

3.4.2. Deflection measurements

The plate tip deflection response over time was measured using high-speed video (HSV) tracking. Fig. 13c and d show the different measurement locations annotated on the *HSV* camera views. Tip deflection and twist were generated by measurement of the locations *S1* and *S2* from *HSV1*, while the beam bending behaviour was obtained from locations *LE1* - *LE8* in the *HSV2* footage. Measurements were taken at $0.5ms$ intervals from the HSV footage for each of these displacement tracking locations. Translational displacements were measured along the global gas-gun $\alpha-$ axis. Plots of tip deflection from locations *S1* and *S2* are given in Fig. 18a and b.

The overall beam deflection response at maximum negative deflection (- ve $\alpha-$ axis direction) and subsequent maximum reversed deflection (+ ve $\alpha-$ axis direction) from the points *LE1* - *LE8* along the

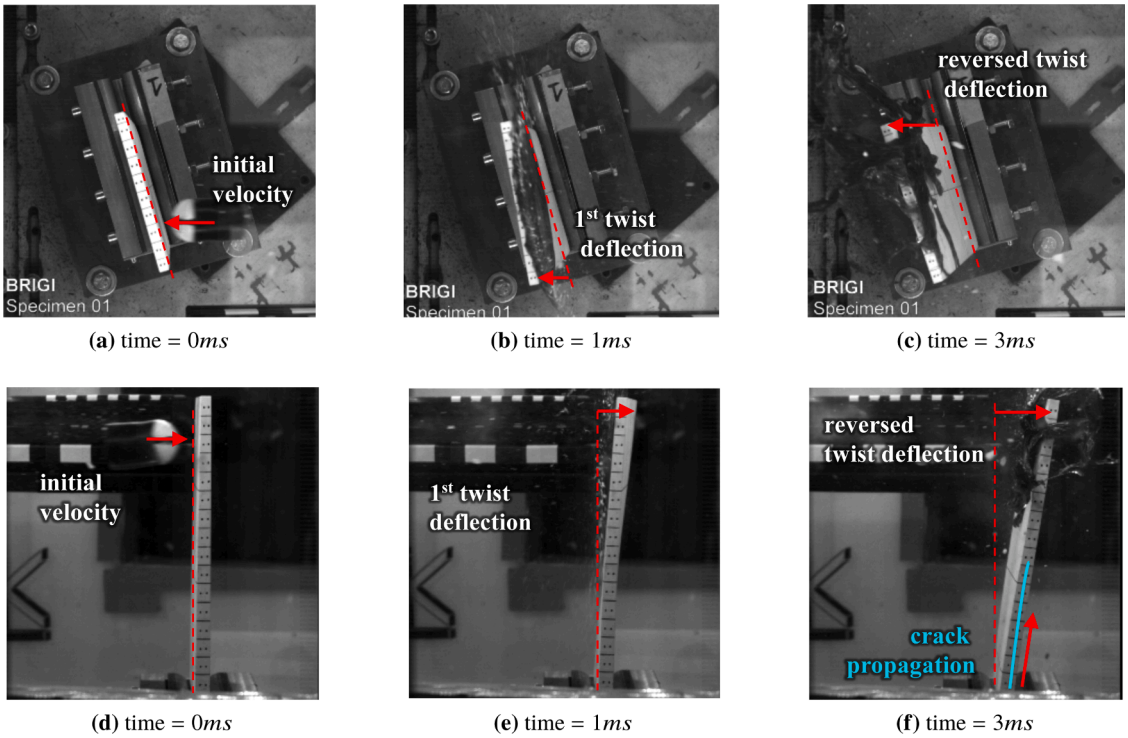

(a) time = $0ms$ **(b)** time = $1ms$ **(c)** time = $3ms$

(d) time = $0ms$ **(e)** time = $1ms$ **(f)** time = $3ms$

Fig. 15. Typical dynamic response (case *CP1* with $V_i = 145m/s$) viewed from both *HSV1* (top) and *HSV2* (bottom), showing transverse deflection and corresponding crack propagation behaviour.

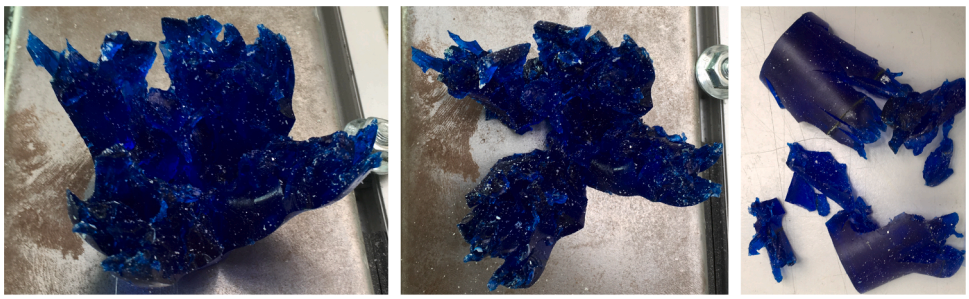

(a) *CP1* (b) *CP1* (2nd view) (c) *CP2*

Fig. 17. Retrieved gelatine from cases *CP1* (Fig. 17a and b) and *CP2* (Fig. 17c), both using a test velocity of $V_i = 145m/s$, showing gelatine damage and intact nature of projectiles post-impact.

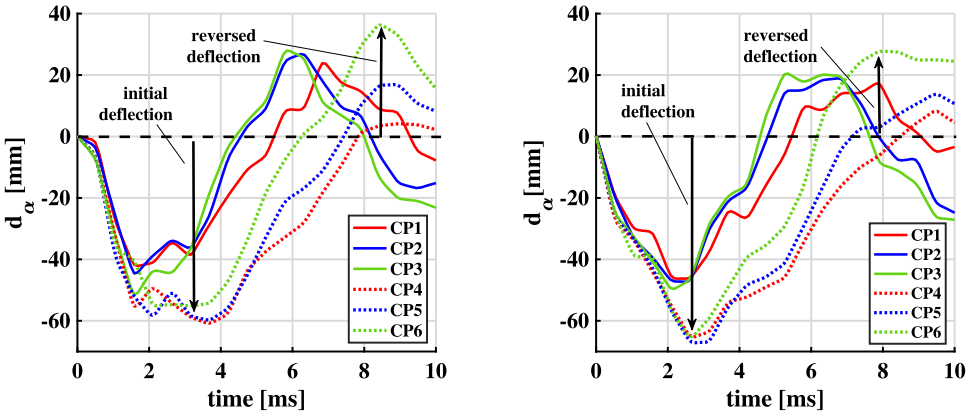

(a) *S1* (b) *S2*

Fig. 18. $\alpha-$ axis tip displacements from tests CP1 - CP6 on unpinned laminates showing data taken from point *S1* (a) and points *S2* (b) with points of initial and reversed full deflections highlighted.

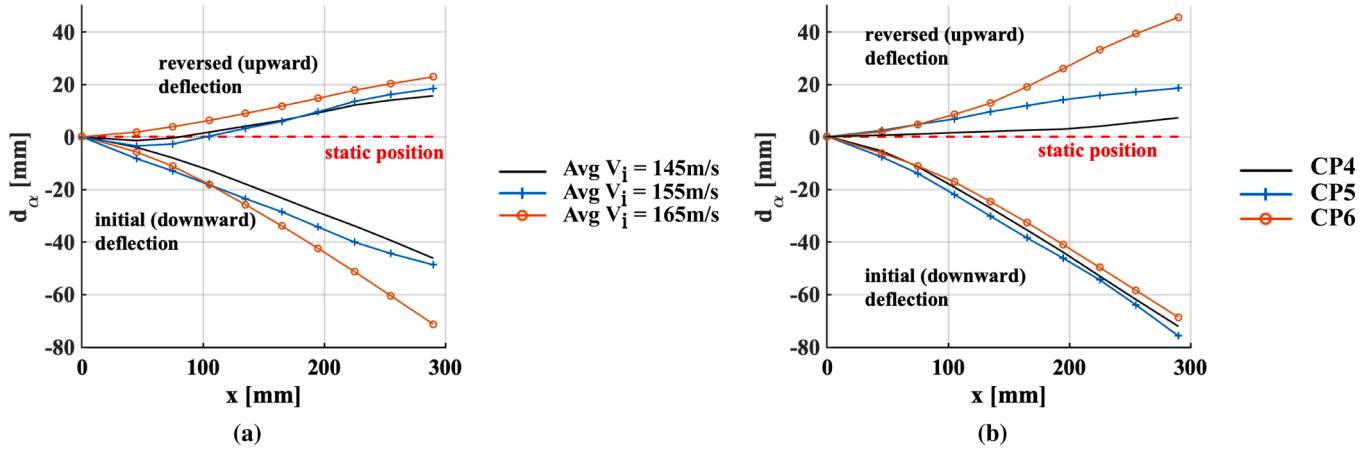

(a) (b)

Fig. 19. Variation in the $\alpha-$ axis displacement of each point *LE1* - *LE8* showing a side-on profile view of the minimum and maximum displacements across all points in time; (a) shows average results observed at each distinct test speed and (b) shows results for each test (CP4 - CP6) at the ultimate test velocity $V_i = 165m\ /s$.

span in *HSV2* is given in terms of the averaged result measured for each V_i in Fig. 19a, and for each distinct test undertaken at the final test velocity of $V_i = 165m/s$ in Fig. 19b. Figure 20 shows the twist calculated from the $\alpha-$ axis displacements of points *S1* and *S2* where this is considered positive for anti-clockwise motion around the specimen local $x-$ axis when viewed from tip to root. Figure 20a shows the average twist calculated from results at each test velocity, while Fig. 20b shows each individual result for the cases at $V_i = 165m/s$. In order to better contextualise the tip deflection and twist plots, images of cases at each test speed used are presented at their static position and at their maximum initial and reversed deflections - from the perspective of both *HSV1* and *HSV2* - in Figs. 21 and 22 respectively.

There appears to be little change in behaviour between tests *CP2* and *CP3*, which show a very similar displacement response and yet were conducted at two different speeds of $V_i = 145m/s$ and $155m/s$ respectively. Conversely, tests *CP1* and *CP2* were both carried out at $V_i = 145m/s$ and yet exhibit greater differences in their deflection responses. There are also no significant differences in the projectile masses or laminate thicknesses measured before each test as noted in Table 1. It is possible that there is some sensitivity of the test results to even minor

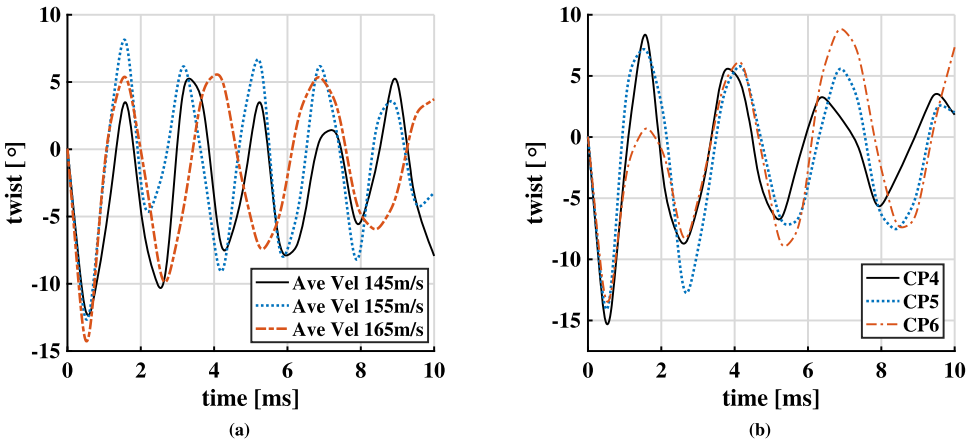

Fig. 20. Specimen twist extracted from the difference in tip displacements from points *S2* and *S1*, with twist being taken as + ve anti-clockwise when viewed along the specimen $x-$ axis from tip to root. (a) shows the twist values averaged across all tests at each test velocity V_i (145, 155 and 165m/s) and (b) shows the twist values for each individual test at $V_i = 165m/s$ (CP4, CP5 and CP6).

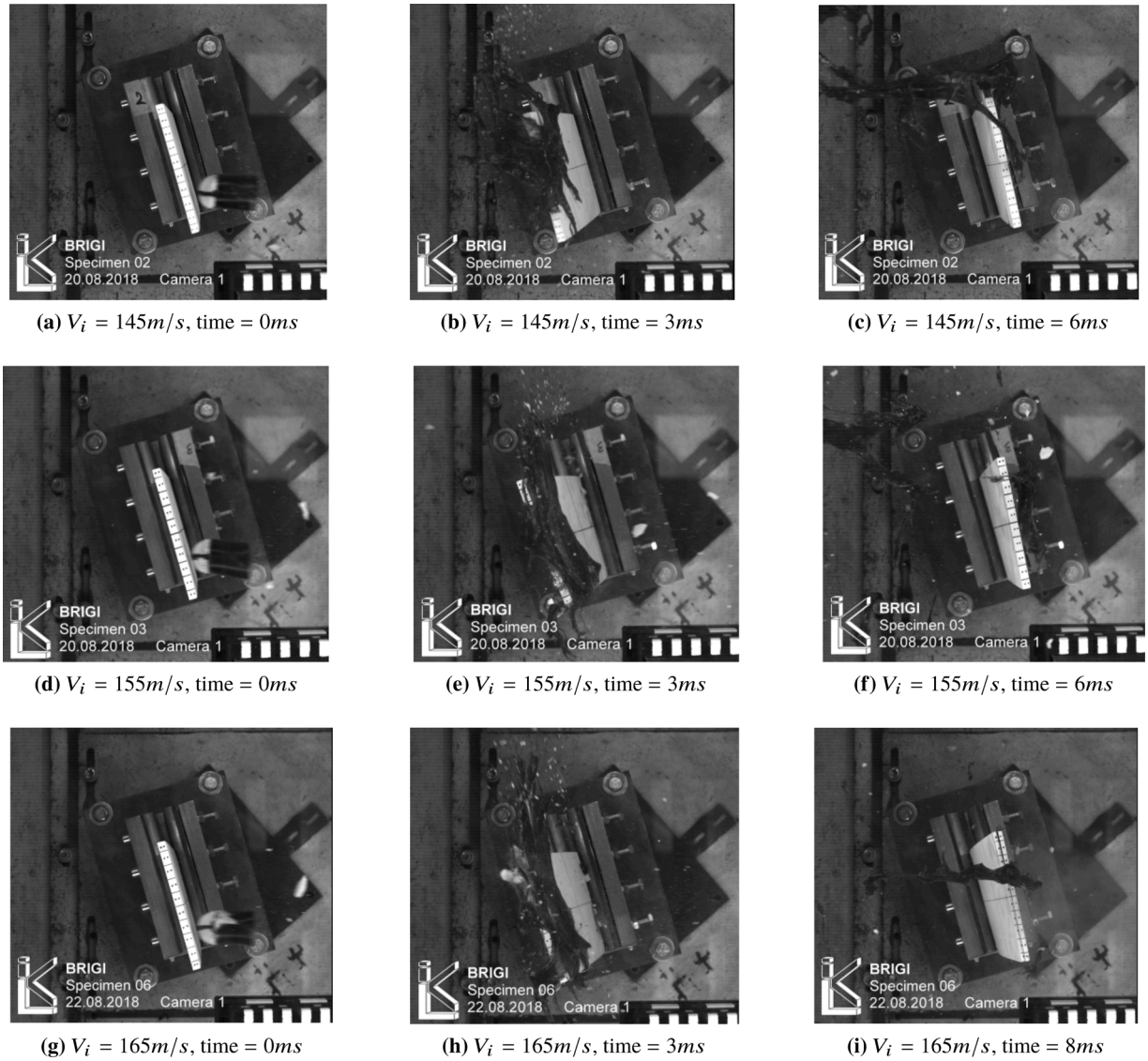

(a) $V_i = 145m/s$, time = $0ms$ **(b)** $V_i = 145m/s$, time = $3ms$ **(c)** $V_i = 145m/s$, time = $6ms$

(d) $V_i = 155m/s$, time = $0ms$ **(e)** $V_i = 155m/s$, time = $3ms$ **(f)** $V_i = 155m/s$, time = $6ms$

(g) $V_i = 165m/s$, time = $0ms$ **(h)** $V_i = 165m/s$, time = $3ms$ **(i)** $V_i = 165m/s$, time = $8ms$

Fig. 21. Dynamic response behaviour for three cases *CP2* ((a)–(c)), *CP3* ((d)–(f)) and *CP6* ((g)–(i))) at $V_i = 145m/s, 155m/s$ and $165m/s$ viewed from *HSV1*.

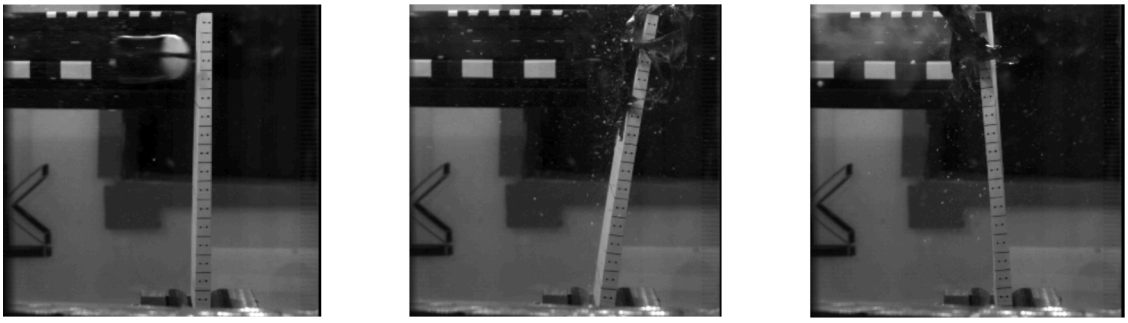

(a) $V_i = 145m/s$, time = $0ms$ **(b)** $V_i = 145m/s$, time = $3ms$ **(c)** $V_i = 145m/s$, time = $6ms$

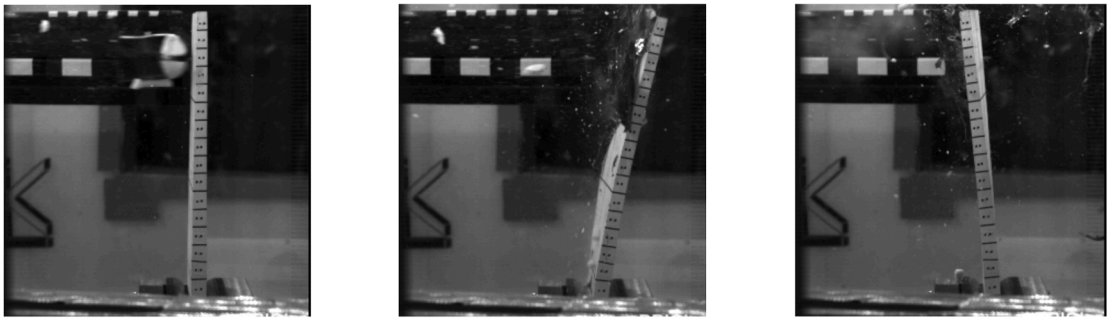

(d) $V_i = 155m/s$, time = $0ms$ **(e)** $V_i = 155m/s$, time = $3ms$ **(f)** $V_i = 155m/s$, time = $6ms$

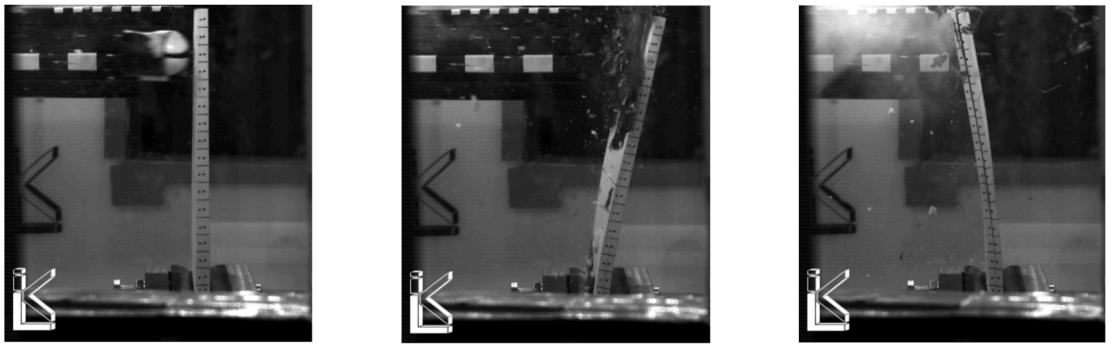

(g) $V_i = 165m/s$, time = $0ms$ **(h)** $V_i = 165m/s$, time = $3ms$ **(i)** $V_i = 165m/s$, time = $8ms$

Fig. 22. Dynamic response behaviour for three cases *CP2* ((a)–(c)), *CP3* ((d)–(f)) and *CP6* ((g)–(i))) and *CP6* at $V_i = 145m/s, 155m/s$ and $165m/s$ viewed from *HSV2*.

changes in the test parameters such as projectile mass & velocity, and it is notable that for tests using ballistic gelatine, the projectile properties may vary with the environmental conditions which could influence differences in the results.The tests were carried out over a number of days, with no deliberate control over the time of testing, e.g. morning vs. afternoon. Although there was some minor day to day fluctuation, the temperature was measured in the laboratory across the tests, and no substantial variation was noted. However, it is likely that the delamination condition of each laminate during the test has the largest effect on the deflection results, and is considered further in the following section.

3.4.3. Delamination

Figure 23 shows the ultrasonic C-scan results for the delamination in all specimens. Analysis of the ultrasonic C-scans of the pristine laminates taken before each test showed no evidence of any delamination or other damage. It is evident that tests *CP2* and *CP3* have the least delamination area, while the specimens *CP1* and *CP4-6* are significantly more delaminated. As previously highlighted, the differences in deflection behaviour shown across Figs. 18–22 are likely to be related to the differences in the amount of delamination occurring in each specimen. For the more intact specimens, the response is characterised by smaller deflections and initial bending deflections that are quickly reversed. Twist in cases where specimens remain more intact tends to reduce over time. For tests which show greater delamination, there is a tendency for the displacement result to increase over time as indicated in the analysis of HSV footage and this appears to happen after the onset of crack initiation and initial propagation. Twist in cases with substantial levels of delamination seems to either remain large or increase over time. The time-displacement relationships suggests that once the specimen reaches a certain tip displacement, delamination initiates and quickly propagates, causing a loss of stiffness which then causes subsequent further displacement, etc. There is also an increase in the period of the deflection cycle for more delaminated specimens. Overall, this behaviour suggests a strong link between delamination within each specimen and the observed deflections.

Considering the data shown in Table 1 and the delamination profiles of the plate area shown in Fig. 23, it is clear that the delamination area A_d is scalable depending on the test velocity used. Figure 25 shows the *normalised delamination area* - the amount of delaminated surface area A_d measured from the 2-D C-scan profile relative to the overall specimen in-plane area - calculated using $A_d =$ (delaminated area/total specimen area) for each of the tests. Test *CP1* shows a much larger amount of delamination than tests *CP2* or *CP3*, with a clear outline of the projectile imprint indicating local delamination has occurred near the impact

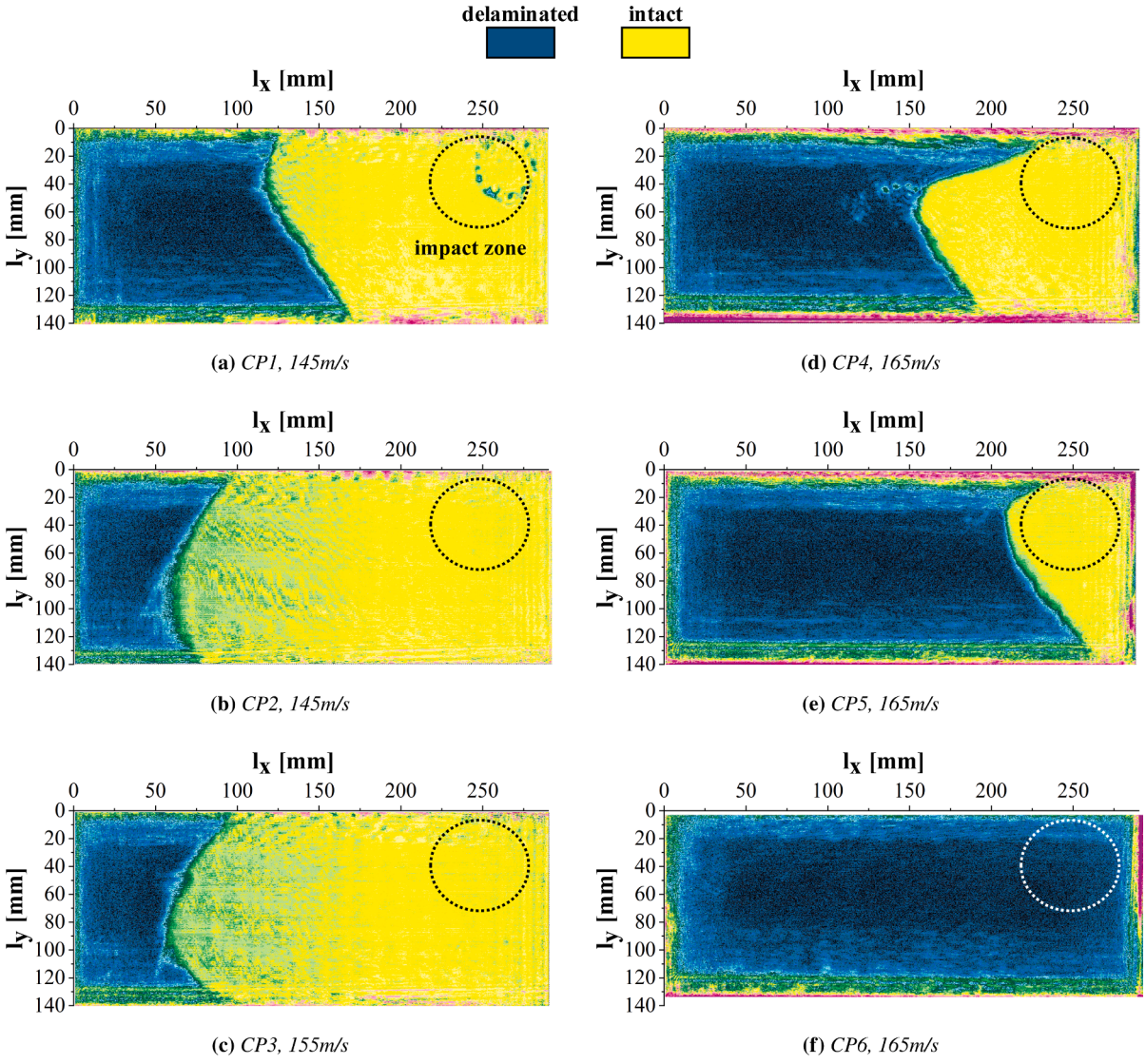

Fig. 23. C-scan plots of delamination for unpinned laminates *CP1 - CP6*, showing region of impact. The specimen root corresponds to $l_x = 0mm$, the visible edge in *HSV1* corresponds to $l_x = 290mm$ and the visible edge in HSV2 corresponds to $l_y = 140mm$.

zone. However, tests *CP2* and *CP3* conducted at different speeds show virtually no difference in the delamination result. Considering the laminate thicknesses, gelatine mass and velocity as detailed in Table 1 for the tests, there appears to be no significant discrepancies. It is therefore assumed that *CP1* is an outlier and it is not taken as standard behaviour for a test shot at $V_i = 145m/s$.

Tests *CP4-6* use a test velocity of $V_i = 165m/s$. From the measured velocities in Table 1 the gas-gun reproduces this velocity to within $\pm 2m/s$. However, from the delamination C-scans in Fig. 23, the test result is clearly highly sensitive to even slight changes in the test environment and parameters or specimen to specimen variation.

Examination of the specimens after testing shows that there is one predominant delamination interface close to the mid-plane of the

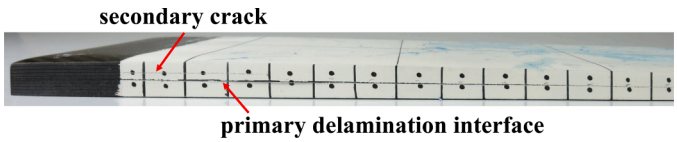

Fig. 24. Photograph taken post-impact showing evidence of a large, primary crack close to the mid-plane from test CP5; a small, secondary delamination has also been highlighted.

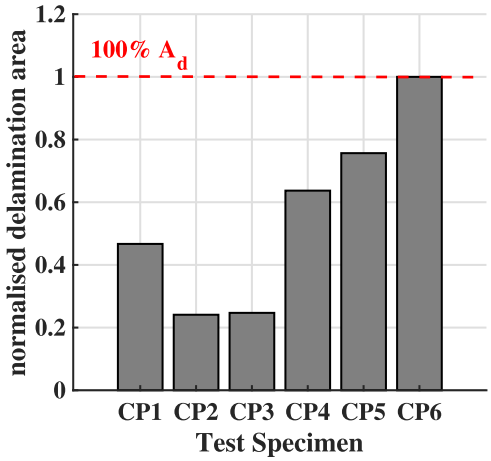

Fig. 25. Normalised delamination area A_d as a fraction of the total specimen in-plane area (A_d = delaminated area/total specimen area).

laminate and this is shown for test *CP5* in Fig. 24. Delamination primarily occurs at the same or very similar through thickness location during each test, which is just below the mid-plane. A number of secondary cracks are visible in certain tests which are generally confined to, or just ahead of, the region where the fixture and the laminate are in contact. Subsequent sectioning of the laminates has shown that these cracks do not extend far into the laminate away from the edge. The secondary delaminations may be considered a result of the high levels of bending in the root region and should not affect the efficacy of the test. In fact, secondary delaminations in this region could act as stress relief on the highly-stressed root region during the critical initial bending deflection.

The substantial variation in delaminated area across the tests performed at $V_i = 165m/s$ from a minimum of $A_d = 64\%$ to a maximum of $A_d = 100\%$ could be attributed to various factors. As mentioned previously, no C-scan results taken prior to testing showed any sign of major damage to any of the laminates, for example, delamination due to waterjet cutting or acquired during transit. It can therefore be ruled out that existing delamination in some laminates caused a difference in the delamination results due to impact. The environment in the test chamber was not temperature-controlled or under vacuum, and so it is possible that minor fluctuations in environmental conditions may have generated some differences in the responses, but conditions other than environmental temperature were not measured. Gelatine behaviour has been shown to be relatively consistent so long as temperature is maintained below a certain level, and this level was monitored and not exceeded during testing. The numerous ply-drops contained in each specimen may have contributed to the variation in the results, with minor differences in transverse normal stresses at the different ply drop locations providing many different drivers for delamination initiation and propagation. It is however clear that a velocity threshold for obtaining full delamination exists, with there being virtually no difference in impact velocity between test CP4, $A_d = 64\%$ and test CP6, $A_d = 100\%$, suggesting that the test velocity of $V_i = 165m/s$ sits almost exactly on the velocity threshold for this specific test configuration. As the delamination is confined generally to a single primary interface, and variation in the delamination result is from partial (64% A_d) to full (100% A_d) delamination, this behaviour is seen as fulfilling of the requirements set out in Section 1. It is acknowledged that performing more test repeats would reduce the level of scatter in data, however, the three repeats undertaken at the critical velocity of $165m/s$, in a relative complex and time consuming test such as this, were felt to be sufficient to give good confidence in the results.

3.4.4. Gelatine behaviour

The behaviour of the gelatine during the test is complex. Detailed analysis of this behaviour is considered outside the scope of this study, however it is useful to examine the gelatine deformation as this will affect the laminate response during the test. The *CP1* case is examined further here, based on a moderate level of delamination ($A_d = 47\%$). Figure 26 shows a comparison of the gelatine motion during the test for the *CP1* experiment from *HSV1*.

Initial gelatine behaviour ($t \leq 0.8ms$) in the experiment (Fig. 26a–c) shows a rapid deformation to a become a very flat mass, spreading across a large amount of the laminate upper surface. During this time period, it appears that the gelatine remains a single mass and does not fragment into different parts (shown previously in Fig. 17). It moves transversely across the surface of the laminate (from tip *S2* to *S1*) before then departing the surface. The gelatine remains on the surface until the full reversed bending deflection of the laminate (not shown in the images). Any fragmentation of the gelatine projectile only seems to occur once it departs the surface. There appears to be a significant amount of friction between the gelatine and the laminate, and the gelatine begins to depart the laminate surface while the laminate is still in downward bending. Further investigation is needed to determine the mechanisms behind the gelatine behaviour, but this data is useful in informing modelling of ballistic gelatine using e.g. using a smooth-particle hydrodynamic (SPH) material model.

4. Post-test fracture analysis

After testing, the specimen from test *CP5* was sectioned into fracture regions using a diamond saw. Thirteen fracture regions defined across the entire crack surface area, each with an upper and lower fracture surface, were selected, with the location of the fracture regions visualised on the fracture surface in Fig. 27. The fracture regions were given an alphanumeric ID corresponding to the location of the fracture region. The configuration of the upper and lower fracture surfaces is that the *upper* surface corresponds to the impact side, and the *lower* surface corresponds to the opposing side to impact.

4.1. Fractographic features

The primary features which assist in determining the nature of the fracture are found on the upper fracture surface of specimen *CP5*. The features are in the form of *shear cusps*, which protrude outwards from the surface and are caused by microcracking in the matrix material as the crack propagates [23]. Figure 28a shows examples of shear cusps from different regions on the upper fracture surface of *CP5*.

Shear cusps may be used to infer certain crack propagation characteristics such as crack mode-ratio at failure. The out-of-plane *cusp tilt* (Fig. 28) helps to identify mode-ratio, with more vertical cusps

(a) $t = 0.0ms$ **(b)** $t = 0.8ms$ **(c)** $t = 3.2ms$

Fig. 26. Experimental gelatine deformation; (a) - (c) show the experimental gelatine behaviour throughout the laminate deflection cycle for the *CP1* test. Gelatine motion is indicated using *white arrows*.

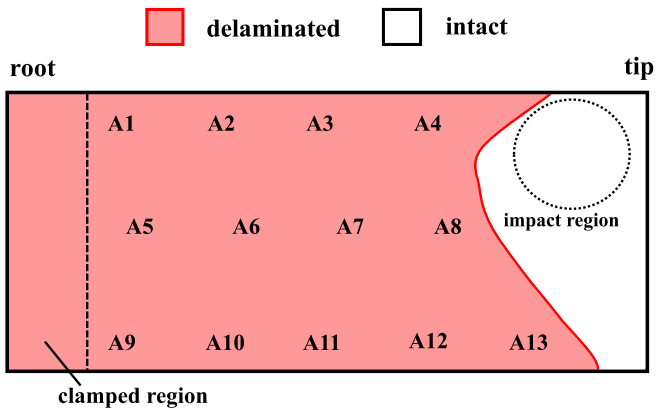

(a) Unpinned (*U/P*) sectioned specimen *CP5* (A)

Fig. 27. Fracture diagram showing the delaminated region overlaid on the specimen geometry with regions e.g. *A1* selected for fracture analysis indicated.

representing a more Mode II crack and flatter cusps representing a more mixed-mode crack.

Figure 28 a–c show samples of shear cusps taken from regions A5, A11 and A13 respectively. Considering the basis for determining mode-ratio outlined above, it can be inferred based on the cusp tilt that the mode-ratio is closer to Mode II in regions nearer the root of the plate, and more mixed-mode as the crack propagates towards the tip.

This general approach was taken during post-test analysis of fracture surfaces in all regions, where qualitative assessments were made regarding the cusp tilt and the possible mode-ratio was estimated. Fracture analysis was performed assuming an entirely vertical cusp represented pure Mode II behaviour, and using this as a reference point. This analysis was used to generate a rough 'failure map' of specimen *CP5*, and this is shown in Fig. 29. It is evident that while this was a qualitative analysis, there is some change in the mode-ratio as the crack progresses from the root towards the tip of the specimen, and this change is a likely reduction in mode-ratio towards more mixed-mode behaviour. The perceived change in mode-ratio is an interesting result and could be attributed to many different mechanisms. Based on the crack progression behaviour shown in Fig. 16, it is possible that as the plate undergoes reversed bending, some crack opening is observed after propagating in Mode II during the initial bending. Other mechanisms could be energy loss due to abrasion as fracture surfaces rub during cracking or higher-order microcracking behaviour. Further work is necessary to determine the exact reasons for this behaviour.

5. Conclusions

A novel test method has been presented for large-scale, high velocity delamination failure performance of sub-element scale composite structures. The test method made use of a light gas-gun and cylindrical gelatine projectile which was used to impact a tapered, cantilevered, pre-preg composite plate at incidence and with high velocity in an off-centre location to invoke large reversed bending deflections. The test method was developed in the context of a requirement to create large-scale delamination. In future work it can be used to benchmark through-thickness reinforcement technologies, such as Z-pins, when encountering delamination failure of sufficient scale to allow for *large-scale crack-bridging*. The test achieved the following outcomes:

- Produced a large, high velocity delamination crack on a predominantly single interface near the mid-plane of the laminate under loading conditions representative of an in-flight impact during take-off or landing;
- Induced delamination initiation and propagation without the use of a pre-crack;
- Avoided any auxiliary failure modes such as fibre-failure near the root;
- Made use of a simple pre-preg specimen design with single-sided taper, manufactured using hand lay-up and autoclave curing with soft-sided vacuum bag tooling and a flat tool surface to minimise manufacturing costs

Impact tests showed that the amount of delamination generated varied between tests and that a test velocity of $V_i = 165m/s$ was necessary to achieve full delamination. However, using this target test

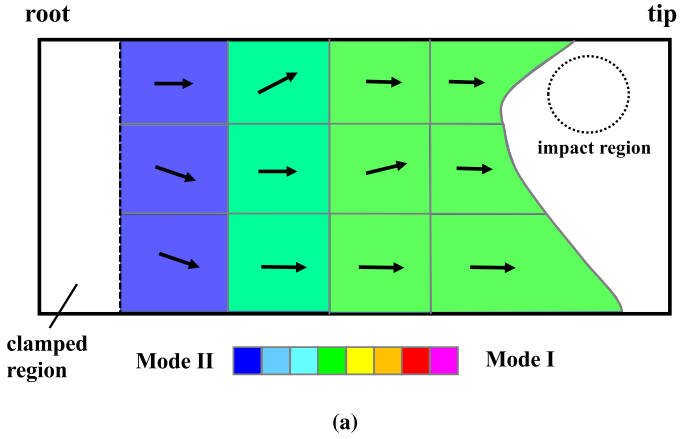

(a)

Fig. 29. Qualitative mode-mixity and crack direction failure map of specimen *CP5*, where the mode-ratio and crack-growth direction are presented. A colour-map is used to represent the severity of the mode-ratio change based on observed features for visualisation purposes *only*.

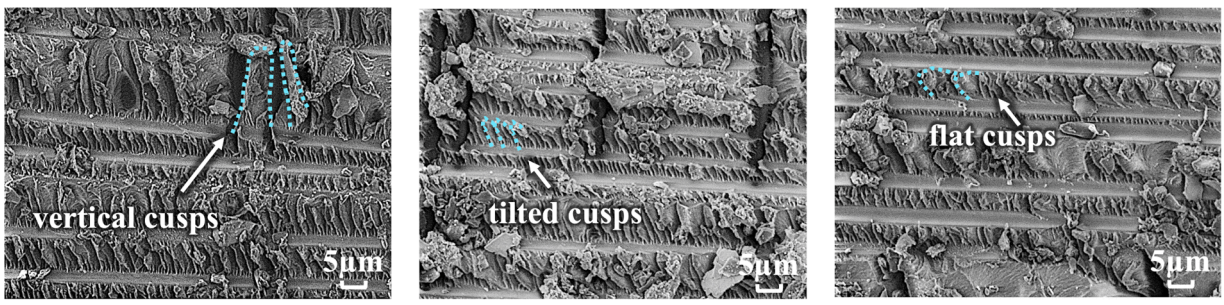

(a) SEM micrograph from region *A5* in the specimen *root region* (1800×)

(b) SEM micrograph from region *A11* in the specimen *mid-span region* (1800×)

(c) SEM micrograph from region *A13* in the specimen *tip region* (1800×)

Fig. 28. Illustration of the variation in cusp out-of-plane tilt with mode-ratio with corresponding SEM micrographs taken from the upper surface in Fig. 27 - a) Near root, b) mid-length and c) near tip.

velocity, the projected 2D delaminated area was found to range between $A_d = 64\%$ and $A_d = 100\%$. Variation in the delaminated area of a particular specimen was found to have a significant effect on the tip deflections observed, with more heavily-delaminated specimens exhibiting greater amounts of deflection. Large variations in delaminated area between specimens tested under very similar conditions was attributed to various factors such as environmental conditions (e.g. temperature) or local specimen variations at ply termination locations acting as a driver for delamination.

Detailed fractographic analysis of the fracture surfaces of a single specimen was performed to investigate the microscopic nature of the fracture behaviour. By estimating the crack mode-ratio using the tilt of the visible shear cusps, it was determined that the crack mode-ratio was likely changing during crack propagation, from more Mode II behaviour near the root to more mixed-mode behaviour nearer the tip.

Inclusion of through-thickness reinforcement such as Z-pins in composite structures may significantly affect failure behaviour. The test method developed and validated in this study is suitable for investigating the performance of TTR at sub-structure length scales and under realistic loading conditions. Aside from potentially testing the performance of TTR, the test in its current configuration may be used to assess the behaviour of different material systems (e.g. thermoplastic or 3-D woven composites) and different stacking sequences, or the test configuration may be altered to reproduce failure or behaviour of a different kind. The test designed in this study represents an important step forward to populating the entire aerospace pyramid of testing [24] and establishing a framework for the future virtual testing of composite structures.

CRediT authorship contribution statement

A.D. Cochrane: Investigation, Validation, Formal analysis, Writing – original draft. **J. Serra:** Methodology, Writing – review & editing, Supervision. **J.K. Lander:** Supervision, Conceptualization. **I.K. Partridge:** Supervision, Funding acquisition. **H. Böhm:** Methodology, Investigation. **T. Wollmann:** Methodology, Investigation. **A. Hornig:** Methodology. **M. Gude:** Supervision. **S.R. Hallett:** Conceptualization, Writing – review & editing, Supervision, Funding acquisition.

Declaration of Competing Interest

The authors declare that they have no known competing financial interests or personal relationships that could have appeared to influence the work reported in this paper.

Acknowledgement

The authors wish to acknowledge the support of Rolls-Royce plc through the Composites University Technology Centre (UTC) at the University of Bristol and through the Lightweight Structures and Materials and Robust Design UTC at the Technische Universitat Dresden. The EPSRC is acknowledged through the Centre for Doctoral Training in Composites Manufacture (grant no. EP/L015102/1) as well as the "Understanding Delamination Suppression at High Deformation Rates in Through-Thickness Reinforced Laminated Composites" project (grant no. EP/M015319/1).

References

[1] Zhu L, Li N, Childs P. Light-weighting in aerospace component and system design. Propul Power Res 2018;7(2):103–19. https://doi.org/10.1016/j.jppr.2018.04.001.
[2] Carti DD, DellAnno G, Poulin E, Partridge IK. 3D Reinforcement of stiffener-to-skin T-joints by Z-pinning and tufting. Eng Fract Mech 2006;73(16):2532–40. https://doi.org/10.1016/j.engfracmech.2006.06.012.
[3] Cui H, Yasaee M, Kalwak G, Pellegrino A, Partridge IK, Hallett SR, et al. Bridging mechanisms of through-thickness reinforcement in dynamic mode I&II delamination. Compos Part A Appl SciManuf 2017;99:198–207. https://doi.org/10.1016/j.compositesa.2017.04.009.
[4] Heimbs S, Bergmann T, Schueler D, Toso-Pentecte N. High velocity impact on preloaded composite plates. Compos Struct 2014;111:158–68. https://doi.org/10.1016/j.compstruct.2013.12.031.
[5] DellAnno G, Treiber J, Partridge I. Manufacturing of composite parts reinforced through-thickness by tufting. Robot Comput Integr Manuf 2016;37:262–72. https://doi.org/10.1016/j.rcim.2015.04.004.
[6] Greenhalgh E, Hiley M. The assessment of novel materials and processes for the impact tolerant design of stiffened composite aerospace structures. Compos Part A Appl SciManuf 2003;34(2):151–61. https://doi.org/10.1016/S1359-835X(02)00188-4.
[7] Standard test method for mode I interlaminar fracture toughness of unidirectional fiber-reinforced polymer matrix composites (ASTM D5528). Tech. Rep. West Conshohocken, PA: ASTM International; 2013.
[8] Fibre-reinforced plastic composites determination of the mode II fracture resistance for unidirectionally reinforced materials using the calibrated end-loaded split (C-ELS) test and an effective crack length approach (ISO 15114:2014(en)). Tech. Rep. Geneva, CH: International Organization for Standardization; 2014.
[9] Standard test method for determination of the mode II interlaminar fracture toughness of unidirectional fiber-reinforced polymer matrix composites (ASTM D7905/D7905M-19). Tech. Rep. West Conshohocken, PA: ASTM International; 2019.
[10] Standard test method for mixed mode I-mode II interlaminar fracture toughness of unidirectional fiber reinforced polymer matrix composites (ASTM D6671/D6671M). Tech. Rep. West Conshohocken, PA: ASTM International; 2019.
[11] Partridge I, Cartie D. Delamination resistant laminates by Z-Fiber pinning: Part I manufacture and fracture performance. Compos Part A Appl SciManuf 2005;36(1):55–64. https://doi.org/10.1016/S1359-835X(04)00180-0.
[12] Rezai A, Cartia D, Partridge I, Irving P. Interlaminar damage resistance of Z-fiber reinforced structural CFRP. Proceedings of the 13th European conference on composite materials. Beijing, China; 2001.
[13] Yasaee AM, Mohamed BG, Allegri CG, Hallett SR. Delamination resistance of through-thickness reinforced composites. Proceedings of the 16th European conference on composite materials. Seville, Spain; 2014.
[14] Sayers KH. Design and analysis methods for soft-body impact on laminated composite material and metal jet-engine fan-blades. Fibre Sci Technol 1974;8:173–206.
[15] NASA Technical report: impact resistance of hybrid composites fan blade materials (NASA CR-134712). Report. Washington, D.C.: Pratt + Whitney Aircraft (for National Aeronautics and Space Administration (NASA)); 1974.
[16] NASA Technical report: impact resistance of composite fan blades (NASA CR-134707). Tech. Rep. Washington, D.C.: National Aeronautics and Space Administration (NASA); 1974.
[17] Mouritz A. Review of Z-pinned composite laminates. Compo Part A Appl SciManuf 2007;38(12):2383–97. https://doi.org/10.1016/j.compositesa.2007.08.016.
[18] Read S.. Test apparatus and method of testing. US Patent 7,845,207, 2010.
[19] Kalwak G, Read S, Jevons M, Petrinic N. Investigation of the delamination characteristics of composite specimens with through-thickness reinforcement using an inertia-constrained soft-body beam bend test specimen. Proceedings of the 16th European conference on composite materials. Seville, Spain; 2014.
[20] Hou J, Ruiz C. Soft body impact on laminated composite materials. Compos Part A Appl SciManuf 2007;38(2):505–15. https://doi.org/10.1016/j.compositesa.2006.02.018.
[21] Miller SG, Handschuh KM, Sinnott MJ, Kohlman LW, Roberts GD, Martin RE, Ruggeri CR, Pereira JM. Materials, manufacturing, and test development of a composite fan blade leading edge subcomponent for improved impact resistance. 26. 2015.
[22] Material data sheet: Hexply 8552 data sheet. Hexcel Corporation; 2016.
[23] Greenhalgh E. Failure analysis and fractography of polymer composites. Woodhead Publishing; 2009.
[24] Military handbook - MIL-HDBK-17-1F: composite materials handbook, volume 1 - polymer matrix composites guidelines for characterization of structural materials. Report. Maryland: U.S. Department of Defense; 2002.